Dislocation movement and hysteresis in Maraging blades

Arianna Di Cintio [a,b], Fabio Marchesoni[c], Maria Ascione [a,d], Abhik Bhawal [e] and Riccardo De Salvo [a]

[a]*LIGO Laboratory, California Institute of Technology, MS 18-34, 1200 E.California Blvd., Pasadena, CA, 91125 USA*
[b]*Dipartimento di Fisica, Università degli studi di Roma "Sapienza", 00185 Roma, Italy*
[c]*INFN-VIRGO Project Dipartimento di Fisica, Universita' di Camerino, I-62032 Camerino, Italy*
[d]*Dipartimento di Ingegneria, Università del Sannio in Benevento, I-82100 Benevento, Italy*
[e]*Arcadia High School, Arcadia, CA, USA*

Abstract

All seismic isolation systems developed for Gravitational Waves Interferometric Detectors, such as LIGO VIRGO and TAMA, make use of Maraging steel blades. The dissipation properties of these blades have been studied at low frequencies, by using a Geometric Anti Spring (GAS) filter, which allowed the exploration of resonant frequencies below 100 mHz. At this frequency an anomalous transfer function was observed in GAS filter: this is one of several motivation for this work.
The many unexpected effects observed and measured are explainable by the collective movement of dislocations inside the material, described with the statistic of the Self Organized Criticality (SOC). At low frequencies, below 200 mHz, the dissipation mechanism can subtract elasticity from the system, even leading to sudden collapse. While the Young's modulus is weaker, excess dissipation is observed. At higher frequencies the applied stress is probably too fast to allow the full growth of dislocation avalanches, and less losses are observed, thus explaining the higher Q-factor in this frequency range. The domino effect that leads to the release of entangled dislocations allows the understanding of the random walk of the VIRGO and TAMA IPs, the anomalous GAS filter transfer function as well as the loss of predictability of the ringdown decay in the LIGO-SAS IPs.

1. Introduction

A study of the dissipation processes in Maraging blades has been carried out by using the Geometric Anti Spring (GAS) mechanism [1].
The GAS filter consists of a set of three radially arranged cantilever blades, clamped at the base to a common frame ring, opposing each other via a central disk. The blades are loaded with a 65 kg weight, as illustrated in figure 1.

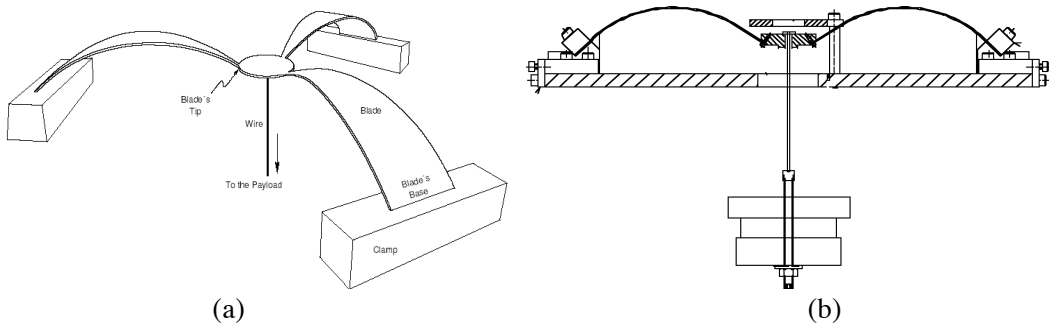

Figure 1: Schematic of a GAS filter: perspective (a) and side view (b). The flat blades are held in 45^0 clamps and pre-stressed.

The clamps can be adjusted to change the blade's horizontal compression, thus generating a theoretically arbitrarily low effective spring constant and resonant frequency, through to the resulting Anti-Spring effect [2].
The GAS mechanism has been used to null 95 to 96% of the spring restoring force at the filter working point, in order to explore hysteresis and any other underlying effects.
The theoretical transfer function of such a filter is

$$H_z(\omega) = \frac{{\omega_0}^2(1+i\phi)+\beta\omega^2}{{\omega_0}^2(1+i\phi)+i\gamma\omega-\omega^2} \quad (1)$$

where ω_0 is the resonant peak frequency, γ is an appropriate viscosity term that, together with the loss angle ϕ, determines the peak width, and β is a mass term which provides the saturation level of the transfer function at high frequencies. Between the resonant and the saturation frequency the amplitude of the transfer function is expected to decrease as $1/\omega^2$
Instead it has been observed that tuning the system at or below 100 mHz, an anomalous transfer function with $1/\omega$ slope appears, in the frequency range 1 to 5 Hz [3].
This anomaly cannot be explained by dissipative phenomena such as the thermoelastic effect, which, for Maraging blades 3.44 mm thick and a heat diffusion coefficient $D_{th} = 5.5\times10^{-6} m^2 s^{-1}$, would peak at a frequency of 0.73 Hz, thus outside the $1/\omega$ region of the anomalous GAS filter transfer function.
This observation, together with many others, such as the hysteresis already observed in GAS filters [4], the tilt hysteresis in Advanced LIGO mirror suspensions [5] and the run-off instability in IPs [6] motivated this study.
The next section will give an overview of the theoretical starting point of this research. In section 3 the experimental set up will be presented and in section 4 we will discuss the data analysis method and the results obtained. Section 5, finally, offers an interpretation of our results, as well as a discussion of future perspective.

2. Theoretical models

Viscosity has been very successful in explaining dissipation properties of materials, but, being proportional to speed, its effects vanish in the zero frequency limit and fails to explain static hysteresis. Low frequency experiments, such as the one presented in [7] and this paper, detect frequency independent losses and static hysteresis.
Hysteresis can be regarded as an effect of spatial disorder [8,9]: even the purest crystals contain a large amount of point (impurities, vacancies) and linear defects (dislocations).
Collective dislocation losses provide the most convincing interpretation of our experimental findings. It is well known that mobile dislocations produce dissipation in metals [10]; until now dissipation was interpreted as the result of the incoherent sum of movements of individual dislocations. In this paper we show how collective dislocation dynamics (avalanches) must be considered to explain the observed properties, including static hysteresis and amplitude dependent losses, of very low frequency mechanical oscillators.
Metallurgy has many dislocation control methods, for example in work hardening dislocations are created in such large numbers that they entangle to the point that their motion is impeded and dissipation suppressed (the material acquires a higher Q-factor and larger elasticity modulus). These trapped dislocations substantially contribute to the mechanical properties of the material: in the presence of low amplitude harmonic stresses, dislocation segments remain pinned inside the crystal and vibrate like ideal elastic strings [11].
In a precipitation hardened alloy, that is our case, as well as in most polycrystalline metals, dislocations can entangle but are not numerous enough to fully interlock, and can disentangle under stress.

Movement of a dislocation can engender domino effects spreading out from an initial point and sweeping through arbitrarily large volumes. Although vibrations of pinned dislocation segments may be extremely short lived, say, in the kHz domain, the domino effects involving large number of dislocations occur on substantially longer time scales. The observed effects we report here are in the time scale of seconds and involve up to the entire size of our flexures of ~ 38 cm. A simple model that closely interpreted our first observations is the Self Organized Criticality (SOC) [12,13]: according to this theory, one can postulate that a certain fraction of the total dislocation network can rearrange by following a self organized pattern, scale-free in space and time (a fractal scenario), thus naturally explaining the residual internal friction at zero frequency and the ubiquitous 1/f noise [14,15].
Combining SOC dislocation models with our measurements we propose the following overall picture. Entangled dislocations form a rigid lattice, which contributes to elasticity. Dislocations can be disentangled by mechanical oscillations, local stresses, or simply thermal fluctuations. If dislocations disentangle, in a domino effect, following a SOC statistic, the material elasticity is reduced and enhanced viscous-like effects are observed. The eventual re-entanglement of dislocations can explain the observed static hysteresis, while the scale-free nature of such processes can explain the unexpected 1/f slope of the GAS transfer function, as well as the presence of 1/f mechanical noise in the system and the other effects that we observed. Dislocation avalanches, finally, cannot contribute to internal friction at high frequencies because they have no time to grow, and lower losses are observed.

3. Experimental setup

The GAS filter has been tuned at low mechanical resonant frequency, tipically 200 mHz (in this experiment 220 mHz and 240 mHz tunes have been used).
The experiment has been performed in a sub-basement laboratory at Caltech, where the main sources of perturbations were due to turbulent air currents and air conditioning thermal cycles. For this reason a box around the GAS filter has been built, made of 2.5 cm thick polystyrene foam panels, which reduced the thermal fluctuations to less than a degree centigrade and deflected most air conditioning wind. However, since the thermal drift of the filter is of the order of one mm/^{0}C, while the measured effect can be on a submicron scale, an active thermal compensation was introduced. This feedback is also necessary to keep the filter at its optimal working point, which corresponds to the height where the Anti Spring effect is maximized and the restoring force of the springs is minimized. For this task an Infinite Impulse Response (IIR) feedback integrator continuously calculates the displacement of the filter from its working point, integrates it and feeds it to a vertical actuator. The actuator [16] is a voice coil mounted coaxial to the load suspension wire.
Similarly mounted, a Linear Variable Differential Transformer [17] sensor was used to acquire the filter displacement signal.
The LVDT calibration, in the linear range of the sensor, was found to be 1.28±0.01 V/mm, while the measured actuator calibration is 26.3±0.3 mN/V.
To further reduce the filter restoring force and resonant frequency, an Electro Magnetic Anti Spring (EMAS) [18] with variable gain has been implemented; it feeds the LVDT signal to the actuator introducing a negative spring constant K_{emas} into the system, to be added to the usual spring constant $K_0 = \omega^2 M$, so the resonant frequency can be expressed

$$f = \frac{1}{2\pi}\sqrt{\frac{K_0 + K_{emas}}{M}} \qquad (2)$$

with a payload M=65 Kg. The EMAS mechanism is able to drive the oscillator all the way to zero frequency or, with positive K_{emas}, to higher frequencies. All the above functions are applied via a Labview control program.

4. Data acquisition and results

4.1 Thermal drift

The LVDT signal was first acquired for several hours, without the thermal feedback: a large amount of thermal hysteresis was observed in the filter movement, as in figure 2a. When switching on the feedback mechanism, which stabilized the filter working point to within a few micron, we expected no residual hysteresis. Instead a similar fractional level of thermal hysteresis has been found in the feedback current that feeds the actuator, as in figure 2b. This observation clearly indicates that hysteresis does not originate from the filter macroscopic movement, but rather from a microscopic dynamics inside the blades.

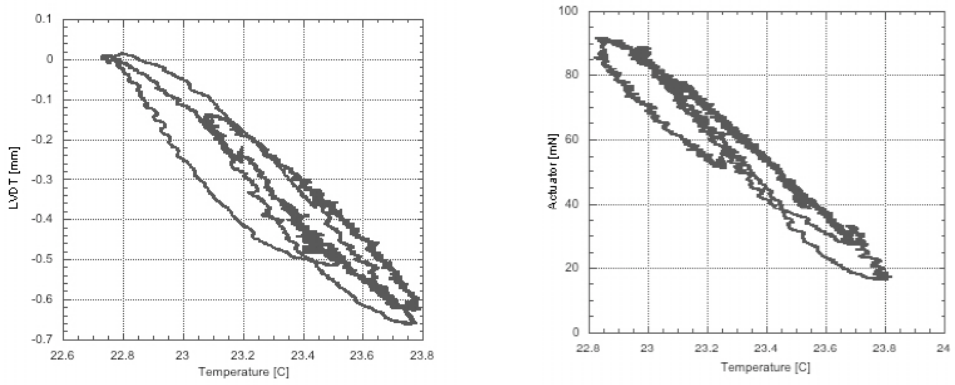

(a) (b)

Figure 2: thermal hysteresis of the filter movement subject to air conditioning thermal fluctuations without feedback (a) and variation of the control current with feedback (b). The data refer to a 10 hours acquisition.

4.2 Hysteresis versus restoring force strength

In order to explore the effects of hysteresis at different filter tunes, excitations of various amplitude and shapes have been applied through the actuator. The measurements have been repeated with alternate sign excitations to cancel thermal drift effects. A thermal feedback time constant much longer than the experiment time scale was used. The measurements were performed at different filter frequency tunes.

With an EMAS spring constant $K_{emas} = 0\,\mathrm{N/m}$, that corresponds to a resonant frequency of 220 mHz, we applied a force to the system, then slowly returned it to zero: we observed hysteresis in the GAS filter displacement, only for alternated sign excitations (figure 3a). Next, we subjected the system to the same force, but abruptly cut it when it reached its maximum, and let the system oscillate freely. No hysteresis has been observed in this case (figure 3b): apparently the system oscillations can delete hysteresis.

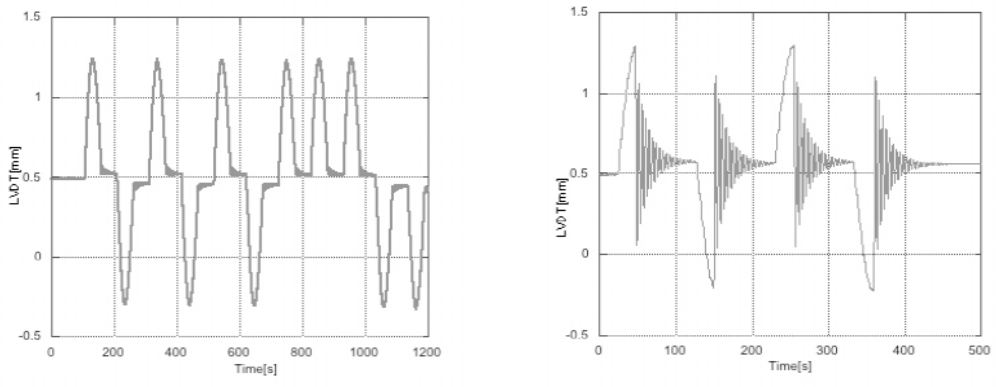

(a) (b)

Figure 3: resonant frequency 220 mHz. Pulse excitation with half period sinusoidal lifting force that grows and then fades at a speed slower than the system response time, non negligible hysteresis is observed (a). Pulse excitation with quarter period sinusoidal lifting force, no hysteresis is observed after the first excitation (b).

The same analysis has been repeated for different K_{emas}, corresponding to progressively lower resonant frequencies. For an EMAS spring constant $K_{emas} = -66.86$ N/m, that provides a resonant frequency of 150 mHz, the springs present such a low Q-factor that the residual oscillations are not sufficient to delete hysteresis in the quarter period excitation (figure 4b to be compared with figure 3b). As for the half period excitation, we found that hysteresis grows rapidly for lower frequency tunes (figure 4a).

The proposed explanation is that elasticity is composed of two parts: the bulk, immutable, provided by the crystalline structure, and a percentage provided by entangled dislocations. The second contribution changes with the dislocation's distribution: its equilibrium point depends on where the dislocation entangle and freeze. The dislocations, mobilized under the pulsed stresses, re-entangle eventually in different equilibrium position, thus explaining the observed hysteresis. The GAS and the EMAS mechanisms reduce the overall restoring force thus enhancing the effect.

The effect is dramatically evident when the system approaches the lowest frequencies, where the restoring force of the crystal lattice structure is almost nulled by the EMAS mechanism (compare figure 3a and 4a). Large excitations triggered run-off instabilities (discussed in section 4.4).

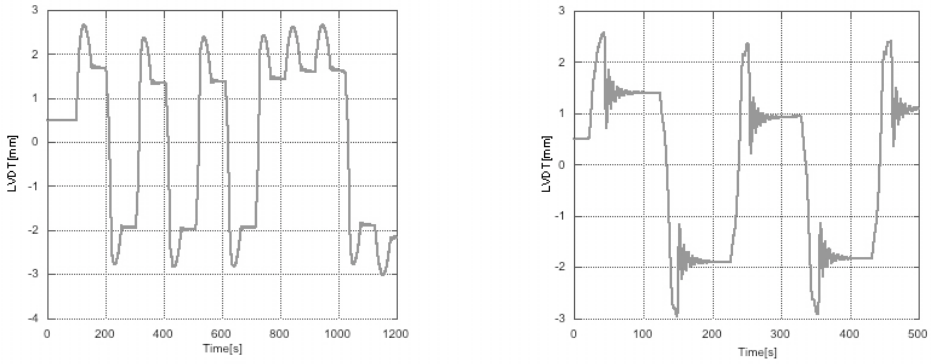

(a) (b)

Figure 4: resonant frequency 150 mHz. Half period excitation (a) and quarter period excitation (b) both show hysteresis. The amount of hysteresis is much larger than the one found with 220 mHz resonant frequency (figure 3a).

4.3 Q-factor

We performed measurements of the system Q-factor for different frequency tunings. The spring was excited by applying a short voltage pulse on the actuator for each EMAS gain setting, and the ensuing ringdown has been monitored. Because of the higher stiffness, we applied 1V excitation amplitudes at higher frequency tune, reducing it to 0.1V at lower frequency tunes, to avoid triggering run-off instabilities (discussed in section 4.4).

Analyzing the ringdown data with a damped sinusoid function we extracted the frequency and lifetime for each system tuning, thus obtaining the Q-factor defined as $Q = \omega\tau$.

The Q-factor should follow a quadratic function of frequency if the losses per cycle are frequency independent [7]; we found the expected quadratic behavior at low frequency, and a deviation from it at frequencies at or above 0.20 Hz, as if a loss mechanism were depressed at high frequencies (figure 5).

In order to verify that the observed departure from the quadratic law was not related to a non-linear control system, the filter's GAS mechanical tune has been softened 23% in stiffness (lowering its resonant frequency from 245 to 222 mHz) and the Q-factor has been measured again for several EMAS gains. The data of the two cases overlap (the two data sets are mixed in figure 5), and the point of departure from the quadratic law is unchanged. This indicates that the deviation from the f^2 law at ~200 mHz is likely a property of the material, and not tune or EMAS dependent. The observed increase of the Q-factor implies strongly reduced losses at higher frequencies; this can be explained if the dissipation process needs a longer time to develop. If the system is slow enough, a limit loss level is reached, corresponding to an hysteretic regime in which dislocation avalanches can fully grow and maximally mobilize, thus giving reason of the time independent dissipation (low Q-factor, quadratic in frequency) observed at low frequencies; at higher frequencies, less dissipation occurs, because there is no time for a full avalanche development, many dislocations are still entangled and cannot contribute to the dissipation processes.

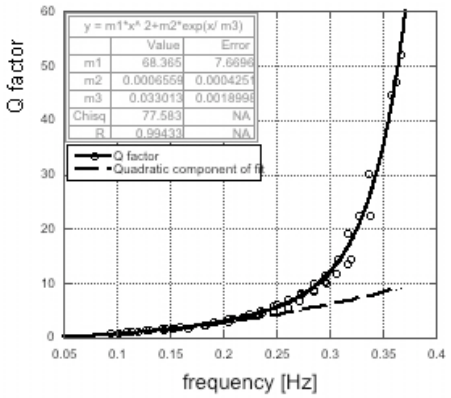

Figure 5: Q-factor of a GAS filter. The data have been analyzed with an exponential profile deviation (solid line) from a quadratic function. The dashed line is the expected quadratic component of the fit, which dominates below 0.2 Hz. Note that if the exponential fit used held all the way, the Q-factor would reach the well-known Maraging Q-factor in excess of 10,000 before 0. 5 Hz.

4.4 Low frequency instability

Exciting the system below 200 mHz we observed that the system occasionally runs away from its equilibrium point, indifferently up or down: large pulses were necessary to destabilize the system at high frequency settings, while at the lowest oscillation frequency achieved, 94 mHz, even a short pulse with amplitude of less than 3 mN (over the 65 kg payload) was able to drive the system into collapse. At lower EMAS gain, ambient perturbations are sufficient to cause the spring's run-off. It is important to remember that a stable oscillator cannot spontaneously destabilize without a failure of Hooke's law of elasticity. Unexplained collapse has been already observed in low frequency systems as different as IPs [6], Virgo [19] and TAMA IP tables, Virgo SA filters, LIGO and TAMA GAS filters [20], etc.. In order to explore the run-off instabilities, the GAS filter has been scanned with increasing negative K_{emas}, i.e. decreasing resonant frequencies, while maintaining the filter at its working point position with a slow position correction integrator. The run-offs start at random directions around 40 mHz, substantially far from the mathematical instability marked by the zero frequency in figure 6a. Evidently the perturbation level in the laboratory is sufficient to impede stability at that low frequency. Note that the initial run-off is slow, much slower than the time constant corresponding to the frequency tune, and then accelerates, as illustrated in figure 6b: this observation seems to indicate that some suddenly-activated, Young's modulus reducing mechanism occurred inside the blades. The effect can be explained if one accepts that the restoring force provided by the crystalline structure is nulled by the GAS and the EMAS mechanisms, and that the system is kept stable only through the metastable restoring force provided by the entangled dislocations. A perturbation that causes some dislocations to disentangle can trigger collapse. To explain the macroscopic run-off of the large payload, the perturbation must propagate to the entire spring's volume. It can be seen as a domino effect in which a single localized event slowly sets in motion avalanches involving a growing number of dislocations in its neighborhood. The collapse happens when a sufficient number of disentangled dislocations stop providing their share of restoring force. Avalanche propagation is not appreciable at higher frequency oscillator tune, where the more rapid oscillation of the stress field limits the development of individual avalanches, thus preventing the domino effect from extending over macroscopic distances. At low frequency dislocation avalanches can grow indefinitely producing observable macroscopic effects.

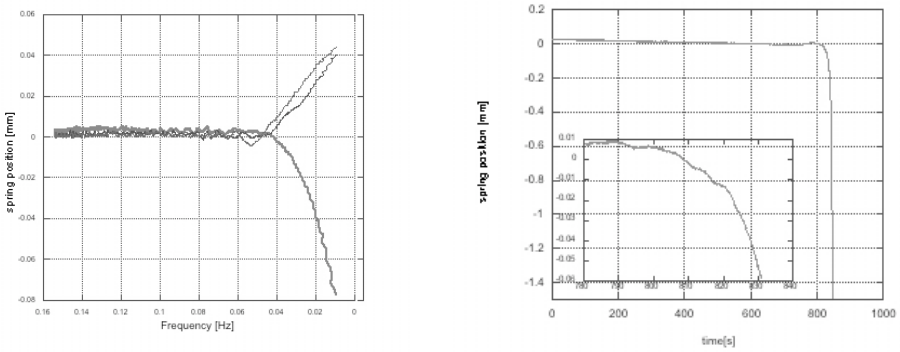

(a) (b)

Figure 6: (a) EMAS gain sweeps with run-offs of the GAS filter starting at about 40 mHz; (b) time evolution and zoom-in of a collapse event. The filter first abandons the equilibrium position very slowly (see insert), then it accelerates. It looks as if an unobserved perturbation had triggered the event by injecting some destabilization energy in the system, and the fall then provides more energy to accelerate the process.

To verify that the process involved in this fall is connected to dislocation avalanches, we wrote a program able to detect the beginning of a run-off with a threshold of 30 mV (~24 μm). The filter has been tuned under 200 mHz, inside the instability region. When a collapse is detected the program temporarily reduced the K_{emas} toward a less negative value, thus slightly increasing the resonant frequency, to give the system more rigidity. When the system has recovered equilibrium the K_{emas} is restored to the original value, following an exponential decay law (figure 7).

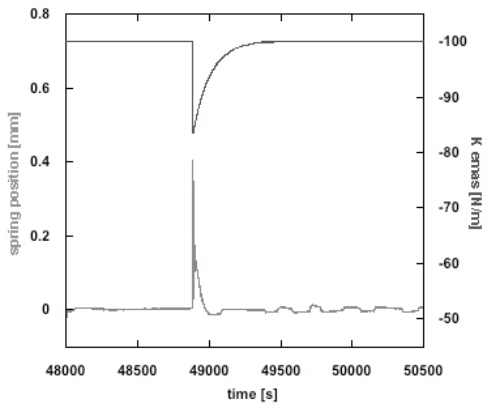

Figure 7: reducing the K_{emas} (top line), in this example from -100 to -80 N/m, the run-off (jump in the bottom line) is stopped. The filter is then slowly returned to its equilibrium position by the integrator; finally the K_{emas} returns to its original value.

4.5 Dissipation and stiffness dependence from amplitude

The stiffness and dissipation measured in forced oscillatory regime were observed to share the same amplitude dependence, proportional to the square root of the oscillation amplitude, a power law typical of SOC systems. We performed two sets of swept sine measurements one made with K_{emas} =0 N/m and one with K_{emas} =-66.86 N/m. In both cases the GAS tune was ~225 mHz. Considering a scenario involving SOC of dislocations, the total elastic constant of the system can be thought as:

$$K_{effective} = K_B + K_A A^x$$

where K_B is a fixed term and $K_A A^x$ is an amplitude dependent term, to account for the stiffness loss due to the fraction of dislocation network disentangled by the motion. The resonant frequency for the M=65kg payload mass thus becomes amplitude dependent according to the formula:

$$f = \frac{1}{2\pi}\sqrt{\frac{K_B + K_A A^x}{M}} \qquad (3)$$

Fitting the swept sine data with the previous function we expect that K_A, indicated as the fit parameter m2 in figure 8, takes a negative value if dislocation disentanglement weakens the Young's modulus.

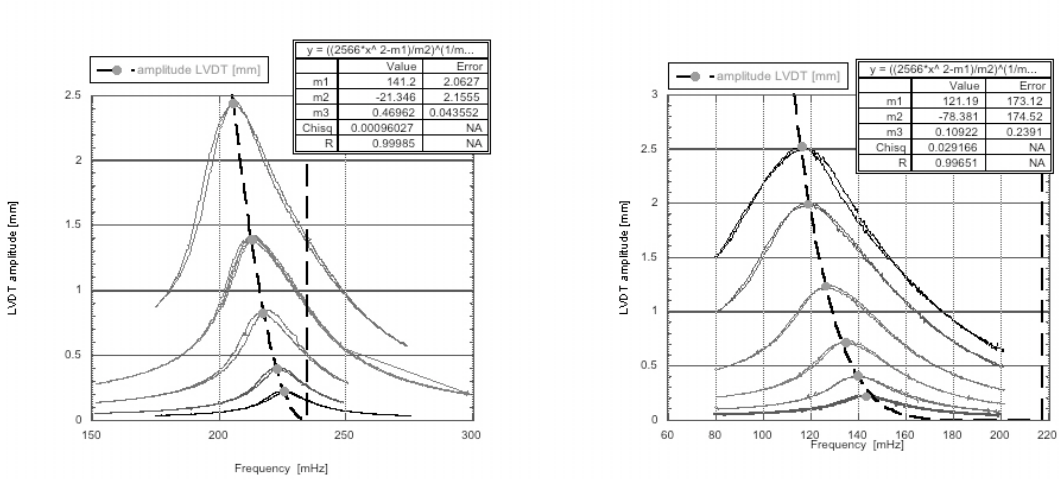

Figure 8: Swept sine response of the system. Each scan was performed sweeping the frequency first up and then down. The scans were repeated with increasing excitation amplitudes. The entire procedure was performed without EMAS, left, and with K_{emas} =-66.86 N/m, right. For each scan we identified the peak value of the resonance, and we applied the formula (3) to fit the position of the peaks.

The fitted value of the amplitude exponent (fit parameter m3 in figure 8) is x=0.5 within less than a standard deviation without EMAS and within 1.7 σ for a K_{emas} =-66.86 N/m. The amplitude-dependent frequency described by formula (3) was also observed in the time domain, studying ring-down measurements.

The assumption that disentangled dislocations weaken the material Young's modulus led us to think that the freed dislocations might cause increased dissipation. The idea was tested studying short sections of long ring-downs and analyzing them with a damped-sinusoidal function to extract the damping time τ as function of the oscillation amplitude A. Fitting the data with the following function,

$$\tau = \frac{1}{d_0 + \delta A^y} \tag{4}$$

where d_0 is the intrinsic dissipation of the material and δA^y describes a possible contribution from the disentangled dislocations, an amplitude exponent of 0.544±0.037 has been found, only 1.2 σ from the 0.5 value (fit parameter m3 in figure 9).

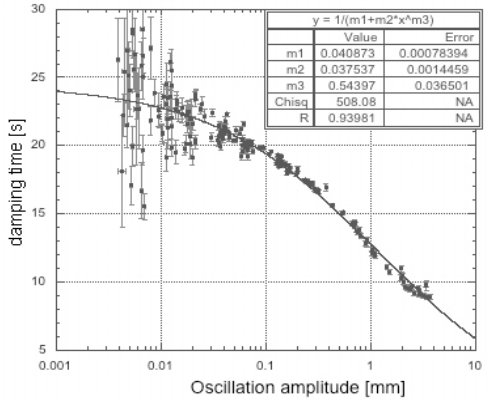

Figure 9: Ring-down lifetime versus amplitude, fitted with a "viscous" term with a power law dependence from the oscillation amplitude.

The fact that the observed loss of Young's modulus and a corresponding increase of dissipation follow the same power law give a strong indication that the two effects share the same source, most likely disentangled dislocations.

5. Conclusion and future perspective

Static hysteresis was the first indicator of something shifting inside the material. That and the previously observed 1/f transfer function of the GAS filter were explained in terms of SOC dynamics of entangled/disentangled dislocation. An avalanche dominated 1/f noise, in excess of that predicted by the fluctuation dissipation theorem, is expected at low frequencies. Individual dislocation avalanches can merge into a single plastic flow causing partial or total collapse. Dislocation avalanches also cause random walks of quiescent mechanical systems. At higher frequencies (>0.2Hz) we may be observing a different scenario. Disentanglement has no time to complete and a large fraction of the dislocations remains inactive. IP or GAS filters tuned at high frequency show well-understood damped behaviors. This may be the case of most experimental internal friction apparatuses, which are typically tuned at relatively high frequency, where dislocation collective effects are negligible. Therefore, extrapolating the result of a measurement to lower frequencies and considering only the thermal noise contribution, may lead to gross underestimation of the low frequency losses and noise. The surprising behavior observed in Maraging steel may actually be typical of most, if not all polycrystalline metals at sufficiently low frequencies. Further studies of loss mechanism are necessary to better understand and control the mechanical noise of future low-frequency interferometers, and of those presently under construction.

The presented results indicate that the most promising avenue will be to study materials or processes that would either stabilize the dislocations, or at least eliminate their collective effects. New materials and processes need to be explored to design the seismic isolation of third generation, lower-frequency GW interferometers.

Glassy materials (metals or ceramics) that do not contain dislocations may be the ultimate materials for seismic attenuation filters and inertial sensors, but need to be studied in depth, as different loss mechanisms like shear bands may still spoil their performance.

Aknowledgements

We would like to thank Christian Cepeda and John Miller for their help in making these measurements possible.

The authors gratefully thank the National Science Foundation, cooperative agreement number PHY-0823459. This document has LIGO number LIGO-P0900028-v2.

References

[1] DeSalvo R 2007 *J. Comput. Nonlinear Dynam.* **2** 290-98
[2] Cella G *et al.* 2005 *Nucl. Instrum. Methods Phys. Res. A* **540** 502-19
[3] Stochino A *et al.* 2007 *Nucl. Instrum. Methods Phys. Res. A* **580** 1559-64
[4] DeSalvo R *et al.* 2005 *Nucl. Instrum. and Meth.* **538** 526-37
[5] Greenhalgh J and Wilmut I 2008 *LIGO Technical Report* LIGO DCC T080033-01-K
[6] Saulson P *et al.* 1994 *Rev. Sci. Instrum.* **65** 182-91
[7] Kimball A L and Lovell D E 1927 *Phys. Rev.* **30** 948-59
[8] Ziman J M 1979 Models of disorder, *CUP Cambridge UK*

[9] Nowick A S and Berry B S 1972 Anelastic Relaxation in Crystalline Solids, *Academic New York*
[10] Hirth J P and Lothe J 1968 Theory of Dislocations, *McGraw-Hill New York*
[11] Granato A V and Lucke K 1966 *Physical Acoustics, edited by Mason and Thurston Academic New York* **IVA** 225
[12] Bak P *et al*. 1987 *Phys. Rev. Lett*. **59** 381-84
[13] Bak P *et al*. 1988 *Phys. Rev. A* **38** 364-74
[14] Marchesoni F and Patriarca M 1994 *Phys. Rev. Lett*. **72** 4101
[15] Marchesoni F *et al*. 1994 *Phys. Lett. A* **187** 359
[16] Wang C *et al*. 2002 *Nucl. Instrum. Methods Phys. Res. A* **489** 563-69
[17] Tariq H *et al*. 2002 *Nucl. Instrum. Methods Phys. Res. A* **489** 570-76
[18] Mantovani M and DeSalvo R 2004 *Nucl. Instrum. and Meth*. **554** 546-54
[19] Ruggi P, VIRGO project, private comm.
[20] R&D and various collaborators